TU Delft

Delft University of Technology

Document Version
Final published version

Licence
Dutch Copyright Act (Article 25fa)

Citation (APA)
Yang, R., Mohapatra, S., Chui, A. P. Y., Chen, S. S., & Jong, M.-C. (2026). Transboundary ecological risks and toxicological mechanisms of a fluorinated liquid crystal monomer and aged microplastics. *Journal of Hazardous Materials*, *507*, Article 141802. https://doi.org/10.1016/j.jhazmat.2026.141802

Important note
To cite this publication, please use the final published version (if applicable).
Please check the document version above.

Copyright
In case the licence states “Dutch Copyright Act (Article 25fa)”, this publication was made available Green Open Access via the TU Delft Institutional Repository pursuant to Dutch Copyright Act (Article 25fa, the Taverne amendment). This provision does not affect copyright ownership.
Unless copyright is transferred by contract or statute, it remains with the copyright holder.

Sharing and reuse
Other than for strictly personal use, it is not permitted to download, forward or distribute the text or part of it, without the consent of the author(s) and/or copyright holder(s), unless the work is under an open content license such as Creative Commons.

Takedown policy
Please contact us and provide details if you believe this document breaches copyrights.
We will remove access to the work immediately and investigate your claim.

This work is downloaded from Delft University of Technology.

Journal of Hazardous Materials 507 (2026) 141802

Contents lists available at ScienceDirect

Journal of Hazardous Materials

journal homepage: www.elsevier.com/locate/jhazmat

Transboundary ecological risks and toxicological mechanisms of a fluorinated liquid crystal monomer and aged microplastics

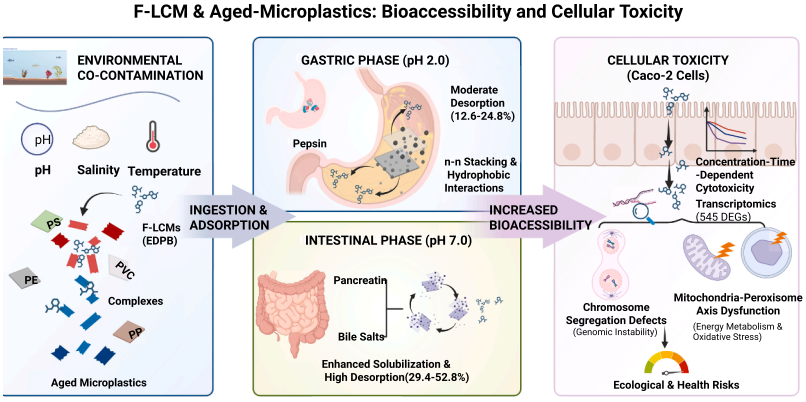
Rui Yang [a], Sanjeeb Mohapatra [b], Apple Pui-Yi Chui [c], Season Si Chen [a,*], Mui-Choo Jong [a,*]

[a] Institute of Environment and Ecology, Tsinghua Shenzhen International Graduate School, Tsinghua University, Shenzhen 518005, China
[b] Department of Water Management, Faculty of Civil Engineering and Geosciences, Delft University of Technology, Delft, the Netherlands
[c] Simon F.S. Li Marine Science Laboratory, School of Life Sciences, The Chinese University of Hong Kong, Hong Kong Special Administrative Region of China

HIGHLIGHTS

- Digestive fluids enhanced EDPB release from aged microplastics.
- Intestinal conditions caused the highest desorption (29.4–52.8%).
- Biomolecules drove the release of EDPB via competitive adsorption and solubilization.
- EDPB-induced cytotoxicity was concentration- and time-dependent in Caco-2 cells.
- EDPB triggered caspase-dependent apoptosis via synergistic disruption.

GRAPHICAL ABSTRACT



ARTICLE INFO

Keywords:
FLCMs
aged-microplastics
gastrointestinal fluid
bioaccessibility
cell cycle

ABSTRACT

Fluorinated liquid crystal monomers (FLCMs) have recently emerged as persistent organic pollutants, while microplastics serve as important environmental carriers of persistent organic pollutants. However, their interactions with aged microplastics and the consequent ecological risks remain a critical blind spot. This study examined the adsorption-desorption dynamics of a representative FLCM (4-ethoxy-2,3-difluoro-4′-(trans-4-propylcyclohexyl) biphenyl, EDPB) on aged polyethylene, polypropylene, polystyrene, and polyvinyl chloride under both abiotic (i.e., environmental) and biotic (i.e., simulated gastrointestinal) conditions. Surface oxidation and increased roughness of aged polymers markedly enhanced EDPB adsorption, through combined hydrophobic attraction and fluorine-mediated dipole interactions. Desorption was strongly medium dependent. In simulated gastric fluid, pepsin facilitated partial release (12.6–24.8%) by disrupting π–π interactions and promoting surface hydration. In contrast, intestinal components induced substantial remobilization (up to 52.8%) via the formation of hydrophobic cavities and micelle-like structures, increasing dissolved EDPB concentrations by approximately 20 μg L^{-1}. This biphasic desorption profile highlights the critical role of intestinal processes in remobilizing adsorbed FLCMs and elevating their bioaccessible fractions. Subsequent cytotoxicity assays in Caco-2 cells showed dose- and time-dependent inhibition of cell viability, with transcriptomic analysis delineating a

* Corresponding authors.
E-mail addresses: season.chen@sz.tsinghua.edu.cn (S.S. Chen), florence.jong@sz.tsinghua.edu.cn (M.-C. Jong).

https://doi.org/10.1016/j.jhazmat.2026.141802
Received 29 December 2025; Received in revised form 19 February 2026; Accepted 15 March 2026
Available online 17 March 2026
0304-3894/© 2026 Elsevier B.V. All rights are reserved, including those for text and data mining, AI training, and similar technologies.

mitochondrial dysfunction–driven cascade. EDPB acts as a metabolic disruptor that impairs mitochondrial energetics and redox homeostasis, triggering downstream genomic instability and cell cycle arrest, which ultimately implicating oxidative stress–mediated apoptosis. This work synthesizes critical insight into the coupled environmental and biological behaviors of FLCMs, revealing their potential as transboundary persistent toxic substances and advancing the understanding of their risks in microplastic-dominated systems.

1. Introduction

Fluorinated liquid crystal monomers (FLCMs) are an emerging class of persistent organic contaminants characterized by biphenyl backbones bearing alkoxy, halogen (notably fluorine), and often cyano substituents. Driven by the rapid expansion of the display panel industry, global production of liquid crystal monomers has risen 2.6-fold from 500 tons in 2011 to over 1300 tons annually [1–3]. Significant quantities of FLCMs have consequently entered the environment via e-waste recycling and disposal, with an estimated 214 tons released in 2017 [4]. These compounds have been detected at high levels in multiple environmental matrices, including 34 species identified in liquid-crystal display disassembly dust (225 ng g^{-1} to 976 μg g^{-1}), and resist removal in wastewater treatment plants [5,6]. The strong C–F bonds and high hydrophobicity (log $K_ow > 5$) confer exceptional persistence and bioaccumulation potential, while fluorine-mediated interactions promote adsorption to hydrophobic solids such as microplastics and enable long-range transport to remote regions, including the Arctic [7,8]. Human exposure has been evidenced by the detection of 38 FLCMs in serum from Beijing residents (median 132.48 ng g^{-1} lipid weight), with epidemiological data linking elevated levels to cardiovascular outcomes, including atherosclerosis [9]. Despite growing recognition of their widespread occurrence and potential health impacts, little is known about how environmental interfaces govern the fate, transport, and biological accessibility of FLCMs.

Microplastics (< 5 mm) represent one critical environmental interface, acting as dynamic vectors for hydrophobic organic contaminants. Global monitoring reveals concentrations up to 452,800 items km^{-2} in the subtropical North Pacific Gyre [10] and 2.55 × 10^4 items m^{-3} in surface waters of the Guangdong–Hong Kong–Macao Greater Bay Area [11]. Notably, e-waste processing zones exhibit microplastics levels 5–27 times higher than non-industrial regions, and form overlapping pollution zones with FLCMs [12,13]. Through high surface area and intrinsic hydrophobicity, microplastics effectively accumulate hydrophobic organic contaminants (log $K_ow > 5$) at surface concentrations 10^5–10^6 times higher than in ambient water [14,15]. For example, polyamide and polyurethane adsorbed bisphenol A at concentrations 10^5-fold higher than ambient environmental levels with desorption rates below 1% [15]. Environmental plastic pellets accumulate polycyclic aromatic hydrocarbons, polychlorinated biphenyls, and polybrominated diphenyl ethers at loads reaching 40.1 μg g^{-1} [16], substantially exceeding background concentrations. Furthermore, microplastics aging through UV oxidation and abrasion introduces oxygenated sites (–OH, –COOH) that modulate surface polarity and matrix brittleness, simultaneously enhancing adsorption and facilitating release under variable physicochemical conditions [17,18]. Once ingested by aquatic organisms, where microplastics are detected in more than 70% of mussels, fish, and crustaceans samples [19,20], digestive surfactants (e.g., bile salts), acidic conditions (pH ≈ 2), and enzymatic degradation further promote contaminant desorption, with reported release rates for persistent organics exceeding 30% [21–24]. These processes elevate the freely dissolved fraction of bound pollutants, facilitating intestinal absorption and enhancing bioaccessibility [25,26]. These combined environmental and biological processes position aged microplastics as both reservoirs and secondary sources of persistent contaminants.

While microplastics and FLCMs co-occur in dietary systems [27,28], their interactive behavior, particularly whether microplastics amplify or mitigate the bioaccessibility of FLCMs, remains unquantified, hindering accurate exposure assessment. The strong C–F bonds and low surface energy of FLCMs may restrict desorption under gastrointestinal conditions, yet the mechanistic influence of microplastic aging and digestive parameters on this process remains unknown. Moreover, the cellular consequences of desorbed FLCMs within intestinal systems remain unexplored. To address these gaps, this study employs 4-ethoxy-2,3-difluoro-4′-(trans-4-propylcyclohexyl) biphenyl (EDPB) as a model and representative FLCM, due to its high detection frequency, environmental relevance, and typical physicochemical properties among FLCMs [9,29]. Adsorption–desorption experiments were conducted accordingly, using aged polyethylene (PE), polypropylene (PP), polystyrene (PS), and polyvinyl chloride (PVC) under simulated gastrointestinal conditions. By coupling desorption kinetics with human colon cancer cell line (Caco-2 cell) assays and transcriptomic profiling, this integrated setup links environmentally mediated microplastic exposure of FLCMs to their cellular-level effects in intestinal epithelium, enabling a mechanistic assessment of their human health relevance and persistent toxic behavior.

2. Materials and methods

2.1. Raw materials

Virgin microplastics, including polyethylene (VPE), polypropylene (VPP), polyvinyl chloride (VPVC), and polystyrene (VPS), which represent over 80% of global plastic production [30] and span non-polar, aromatic, and polar polymer classes, were purchased from Shanghai Run Vast Trading Co., Ltd. (China). Samples were sieved through a 40-mesh screen, and particle size distributions were determined by laser particle analysis. EDPB was purchased from Beijing Enocha Technology Co., Ltd. (China). A 100 mg L^{-1} EDPB stock solution was prepared using high-performance liquid chromatography (HPLC) grade acetonitrile and stored at 4 °C. Pepsin A (35 kDa), bovine serum albumin (BSA, ≥ 98%, 66 kDa), and sodium taurocholate (NaT, ≥ 97%) were obtained from Sigma-Aldrich Co. (MO, USA).

2.2. Simulated aging experiments

Microplastic aging was simulated using an ultraviolet (UV) aging chamber (CEL-LAB500, Beijing Zhongjiao Jinyuan Technology Co., Ltd.) to mimic natural weathering conditions. Microplastic samples (0.2 g) were sonicated in 100 mL ultrapure water within a quartz tube and irradiated at 25 ± 2 °C under a 300 W xenon lamp equipped with a visible-light cutoff filter (λ < 400 nm), providing UV radiation between 200 and 400 nm. Continuous stirring at 200 rpm ensured homogeneous suspension, and water was replenished every 12 h during a 120 h exposure period [31,32]. After irradiation, aged microplastics were rinsed five times with ultrapure water, vacuum-filtered, dried at 45 °C, and stored for subsequent analysis. Surface morphology was examined using scanning electron microscope (SEM, Gemini 300, Carl Zeiss Co., Ltd.). Functional group variations were characterized by Fourier transform infrared spectroscopy (FTIR, Nexus 670, Thermo Fisher Scientific), and particle size distributions were determined via nanoparticle tracking analysis.

2.3. Adsorption and desorption of EDPB from aged microplastics

EDPB-loaded aged microplastics were prepared using a batch

equilibration method. Briefly, aged MPs (0.5 g L^{-1}) were suspended in 5 mg L^{-1} EDPB solutions (pH 6.5) and shaken at 200 rpm in the dark at 25 °C for 120 h, a duration determined by preliminary kinetic studies to ensure equilibrium. Post-incubation, MPs were separated via 0.45 μm filtration. The mass of EDPB loaded onto the MPs (mg g^{-1}) was calculated based on the depletion of aqueous EDPB concentrations. This step simulates environmental contamination prior to ingestion, ensuring MPs were pre-saturated before entering the simulated gastrointestinal system. Detailed isotherm parameters are provided in Text S1 and S5. The selected EDPB concentration (5 mg L^{-1}) and microplastic dose (0.5 g L^{-1}) represent a conservative, upper-bound enrichment scenario typical of pollution hotspots (e.g., electronic waste dismantling areas), rather than average ambient conditions. This design aligns with our ongoing field investigations detecting total LCM concentrations (∑LCMs) of 1.72–4.47 μg L^{-1} in surface waters near such sites. Considering the strong hydrophobic partitioning of FLCMs onto polymers, these conditions facilitate the evaluation of microplastics as contaminant vectors while ensuring sufficient analytical sensitivity for subsequent desorption and toxicological assays.

Desorption of EDPB was examined under conditions mimicking aqueous, cold-blooded, and warm-blooded gastrointestinal environments. Simulated gastric fluid contained 3.2 g L^{-1} pepsin A in 100 mM NaCl (pH 2.0), while simulated intestinal fluid comprised 5.0 g L^{-1} BSA and 10 g L^{-1} NaT in 100 mM NaCl (pH 7.0) [33]. To characterize potential competitive interactions, adsorption isotherms of digestive components (pepsin, BSA, NaT) onto aged MPs were also determined using the Freundlich model. Additionally, the solubility of EDPB in various concentrations of pepsin and BSA/NaT solutions was evaluated to assess solubilization effects. EDPB-loaded aged MPs (loading: 2.11, 2.20, 1.34, and 3.20 mg g^{-1} for PE, PP, PVC, and PS, respectively) were incubated in ultrapure water, gastric media, or intestinal media at 18 °C and 37 °C for 150 h with continuous stirring (200 rpm; 8.0 mg MPs mL^{-1}). Supernatants were periodically sampled, filtered (0.45 μm), and analyzed for EDPB concentration (Text S1). Controls included MPs without EDPB (background) and EDPB solutions without MPs (stability).

To simulate physiological digestion, a sequential desorption assay was performed. EDPB-loaded MPs were first incubated in gastric fluid for 2 h, centrifuged, and resuspended in intestinal fluid for 4 h at 18 °C and 37 °C [34]. Supernatants collected after each stage were analyzed to quantify EDPB release. Physiological parameters (37 °C, enzyme concentrations, residence times) were selected to mimic warm-blooded digestion, providing a conservative upper-bound assessment of FLCM bioaccessibility, defined here as the maximum fraction of EDPB desorbed into simulated fluids available for potential absorption.

2.4. Sorption and solubility experiments

To account for variability in gastrointestinal conditions across species and feeding states [16], desorption experiments were performed under systematically varied parameters, including gastric pH (2.0–7.0), intestinal pH (4.5–9.5), ionic strength (10–200 mM NaCl), and temperature (18–37 °C). Desorption behavior was evaluated under simulated gastric (pH 2.0; 3.2 g L^{-1} pepsin A; 100 mM NaCl) and intestinal (pH 7.0; 5.0 g L^{-1} BSA; 10 mM NaT) conditions. The effects of digestive constituents were further examined by altering pepsin concentrations (0–5.0 g L^{-1}) in gastric fluid and BSA/NaT concentrations (0–7.5 g L^{-1} BSA; 0–15 mM NaT) in intestinal fluid. Complementary sorption assays were conducted using aged microplastics exposed to EDPB in the presence of varying pepsin (0.5–5.0 g L^{-1}), BSA (0.5–5.0 g L^{-1}), and NaT (1.0–6.0 g L^{-1}) concentrations to elucidate microplastic–biomolecule interactions influencing EDPB partitioning under gastrointestinal conditions.

2.5. Cell culture and cytotoxicity assay

Caco-2 cells (ATCC® HTB-37™), derived from human colon adenocarcinoma, were used as an in vitro intestinal epithelium monolayer model to evaluate the cytotoxic effects of EDPB. Cells were cultured in Eagle's minimum essential medium (EMEM; ATCC) supplemented with 20% (v/v) fetal bovine serum (FBS; Gibco) at 37°C and 5% CO_2. Cultures were subcultured every 2–3 days using 0.25% trypsin-EDTA (Gibco) to maintain 80–90% confluence. Caco-2 cells were seeded in 96-well (for cytotoxicity) or 6-well (for transcriptomics) plates at a density of 1×10^5 cells/cm^2. The cells were incubated at 37 °C for 48 h to reach 80–90% confluence, ensuring they were in the exponential growth phase before treatment. To avoid the potential sequestration of hydrophobic EDPB by serum proteins, which could significantly alter its bioavailability, the cells were washed with PBS and subsequently exposed to EDPB at various concentrations in serum-free EMEM for the specified durations. This model focuses on the direct cellular responses to the bioaccessible fraction of the target FLCMs. Monolayer integrity was verified via morphological observations (cobblestone-like structures) and trans-epithelial electrical resistance (TEER $>$ 300 Ω·cm^2) prior to exposure experiments [35].

To specifically assess the hazards of the bioaccessible fraction released from microplastics, cells were exposed to dissolved EDPB solutions. This approach decouples the chemical toxicity of desorbed FLCMs from the potential physical effects of microplastic particles, allowing for a precise evaluation of the 'vector-mediated' risk. Toxic effects of EDPB on Caco-2 cells, including cytotoxicity assessed by the Cell Counting Kit-8 (CCK-8) assay, membrane damage evaluated via lactate dehydrogenase (LDH) release, oxidative stress measured using 2′,7′-dichlorofluorescein diacetate (DCFH-DA) fluorescence, and mitochondrial dysfunction determined by the 5,5′,6,6′-tetrachloro-1,1′,3,3′-tetraethylbenzimidazolylcarbocyanine iodide (JC-1) assay, were evaluated across 24–96 h exposures (50–2000 μg L^{-1}) [36], with full methodologies described in the Supporting Information (Text S2).

2.6. RNA extraction, sequencing, and bioinformatics analysis

To elucidate molecular mechanisms underlying EDPB-induced toxicity in intestinal epithelial cells, transcriptome sequencing was performed on Caco-2 cells exposed to a high-dose group (2000 μg L^{-1}) and an unexposed control. The concentration of 2000 μg L^{-1} was selected based on the peak bioaccessible EDPB levels (1490–3560 μg L^{-1}) measured in our simulated intestinal fluids (Section 3.2.2). This dose represents a realistic upper-bound exposure in the intestinal lumen following ingestion of microplastics from highly contaminated hotspots, where localized release from MPs can temporarily exceed average environmental concentrations via a 'chemical pump' effect. Cells were harvested by trypsinization, and total RNA was extracted using the RNeasy® Plus Mini Kit (Qiagen, Germany). RNA quality was confirmed by NanoDrop 2000 (A260/A280 $>$ 1.8) and Agilent 2100 Bioanalyzer (RIN $\geq$ 7.0). PolyA mRNA was enriched using oligo(dT) magnetic beads, and strand-specific libraries were constructed with the NEBNext® Ultra™ II RNA Library Prep Kit (NEB). Paired-end 150 bp sequencing was conducted on the Illumina NovaSeq 6000 platform (Novogene). Raw data underwent quality control ($Fast_{QC}$), and differentially expressed genes ($|log2FC| \geq 1, padj < 0.05$) were identified using DESeq2 (v1.38.3). Functional enrichment analysis was performed using Gene Ontology (GO) and Kyoto Encyclopedia of Genes and Genomes (KEGG) databases (clusterProfiler v4.8.1). Detailed procedures are provided in Supporting Information (Text S3).

2.7. Statistical analysis

The desorption kinetics of EDPB from contaminated aged-microplastics in gastrointestinal fluids were described by a first-order model as described in Text S4. Two-way ANOVA assessed the effects of pH, salinity, and temperature on EDPB desorption from aged-microplastics. Three independent biological replicates ($n = 6$) were used per group, with data expressed as mean ± standard deviation

(mean ± SD). Statistical analyses were performed using GraphPad Prism (v8.03). Nonparametric tests were employed for non-normal data: Kruskal-Wallis with Dunn's post hoc test for within-group comparisons, and Wilcoxon tests for between-group analyses.

3. Results and discussion

3.1. Physicochemical characterization and EDPB adsorption of aged microplastics

The SEM images revealed that virgin PE, PP, PVC, and PS exhibited smooth surfaces with mean particle sizes of 261, 386, 127, and 129 μm, respectively (Table S1, Fig. 1a). After UV exposure, surface roughness and microcracks developed, and particle sizes decreased to 61–111 μm, corresponding to reductions of 38.8–51.9%. The FTIR spectra indicated pronounced oxidation, reflected by increased intensities of $-CH_2$ (3018/2974 cm^{-1}), C–O/C–O–C (1289/1257 cm^{-1}), and C═O (1750 cm^{-1}) bands [37] (Fig. 1b). The carbonyl index increased significantly ($p < 0.01$) for all aged polymers (PE: 1.35, PP: 1.47, PVC: 2.94, PS: 1.65) compared with the virgin materials (PE: 1.18, PP: 1.05, PVC: 1.09, PS: 1.49) (Table S2). These changes indicate UV-induced photo-oxidation involving C–H bond cleavage and peroxyl radical formation, yielding abundant hydroxyl and carboxyl functionalities [38]. The XPS results corroborated the trend that oxygenated carbon fractions increased across all polymers, with elevated C–O and C═O components and a corresponding decline in C–C/C–H signals (Fig. 1c–d). Collectively, SEM, FTIR, and XPS analyses confirm substantial morphological degradation and surface oxidation of all aged microplastics.

The aged microplastics exhibited markedly higher adsorption capacities for EDPB (PE: 1041.62, PP: 1004.58, PVC: 875.27, PS: 1223.63 μg g^{-1}; Text S5, Figure S1–S2, Table S3–S4). The enhancement is attributed to the combined effects of reduced particle size, increased specific surface area, and the introduction of oxygen-containing functional groups (–OH, –COOH) for the aged microplastics, which promote polar and hydrogen-bond interactions with EDPB [38]. While these surface modifications greatly improve sorptive affinity, adsorption represents only the initial step of contaminant–microplastic interaction. Such enriched microplastic-associated contaminant loads may result in localized exposure levels substantially higher than ambient water concentrations upon ingestion, underscoring the potential for microplastics to act as effective contaminant vectors. Upon ingestion, variations in pH, enzymatic composition, and temperature within gastrointestinal systems can trigger desorption, increasing pollutant bioaccessibility through the intestinal barrier [39]. Therefore, quantifying desorption kinetics under physiologically relevant conditions is critical for elucidating the environmental behavior and ecological risk of microplastic-mediated co-contaminants, such as fluorinated liquid crystal monomers.

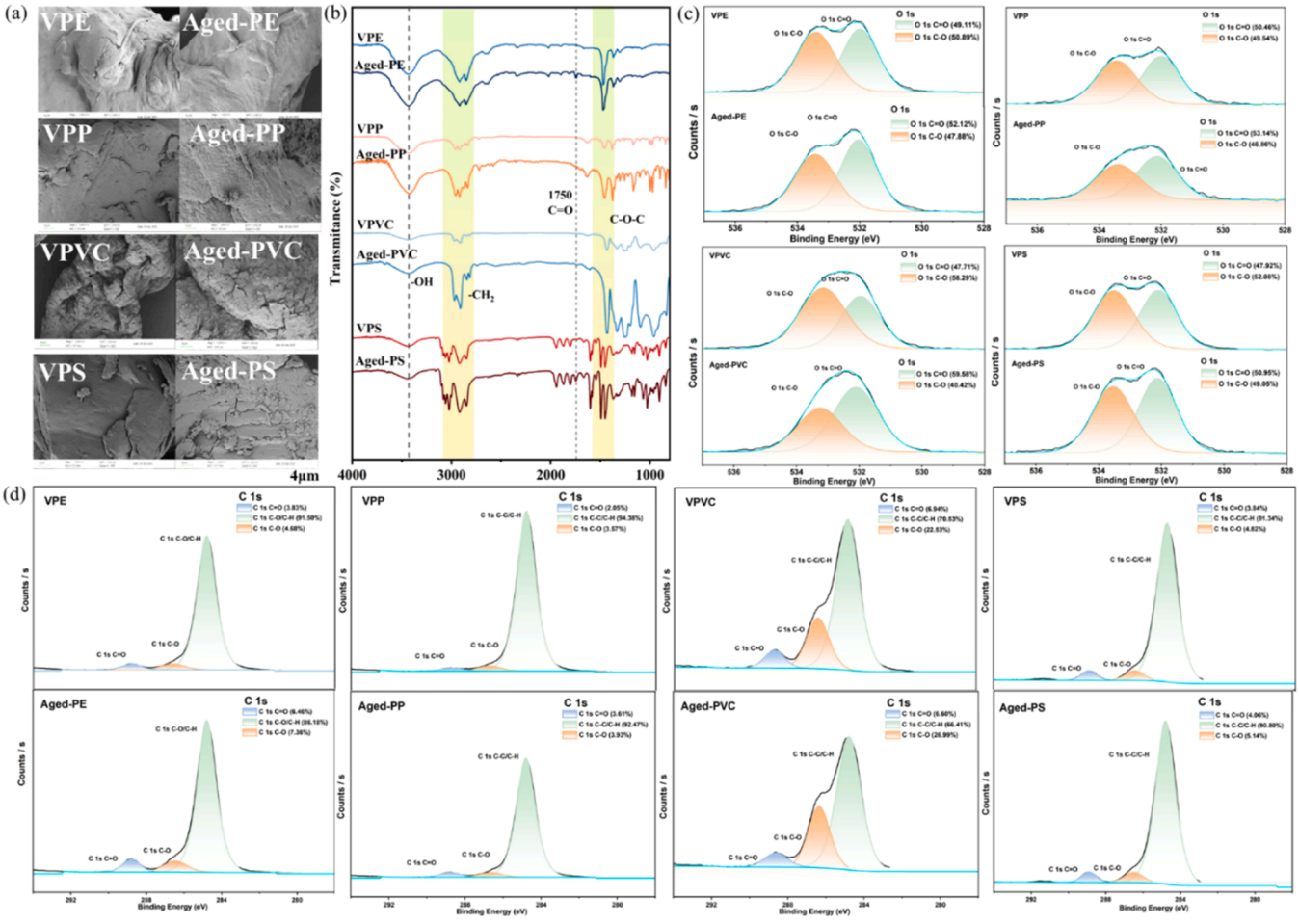


Fig. 1. Surface characterization of aged-microplastics reveals morphological and chemical oxidation changes. (a) SEM image showing morphological changes; (b) FTIR spectroscopy chemical map highlighting oxidation profiles. (c) XPS O 1 s spectra showing the evolution of surface oxidation states, with an increased contribution of carbonyl-related oxygen in aged microplastics. (d) XPS C 1 s spectra revealing the conversion of C–C/C–H to oxygenated carbon species (C–O, C═O) following UV aging.

3.2. Desorption of EDPB in simulated gastrointestinal fluids

3.2.1. Desorption kinetics of composite contamination in a simulated gastrointestinal tract

The desorption kinetics of EDPB from aged microplastics in aqueous and simulated gastrointestinal environments followed a first-order two-compartment model (Table S5), exhibiting a distinct biphasic pattern (Fig. 2). Rapid desorption occurred within the first 8 h, followed by a slower phase approaching equilibrium. Aged PE and PS reached equilibrium within 48 h in gastric and aqueous media, whereas PP and PVC required 72 h. In intestinal fluids, desorption remained incomplete after 150 h, reflecting strong interfacial retention. This kinetic profile mirrors the biphasic release observed for hydrophobic pollutants such as PCBs and PAHs [16,23], consistent with their comparable hydrophobicity (log $K_ow > 5$) and aromatic structures. The fast-desorption fraction (F_{fast}) was notably higher in gastrointestinal media than in water, particularly under warm-blooded conditions (37 °C), indicating that intestinal environments markedly facilitate EDPB remobilization.

Enhanced desorption in gastrointestinal fluids was governed by two synergistic mechanisms: solubilization and competitive adsorption (Figure S3–S4). Intestinal components (BSA and NaT) increased EDPB solubility by forming hydrophobic cavities and micelle-like assemblies, as confirmed by surface-tension measurements (critical micelle concentration: 72.62 mN m^{-1}; Table S6). This micellar solubilization elevated EDPB aqueous concentration by 19.63 μg L^{-1} and reduced interfacial binding energy with aged microplastics [15]. Furthermore, interactions with intestinal components are likely to induce changes in the intrinsic surface properties of aged microplastics. The rapid formation of a "bio-corona" via the adsorption of BSA and NaT may reconfigure the surface polarity of the MPs [40], thereby reducing interfacial tension between the aged polymer and the aqueous medium. This transformation is expected to facilitate the release of hydrophobic EDPB from the MP surface into the micellar phase, consistent with the enhanced desorption observed in intestinal fluids.

Concurrently, pepsin and BSA interacted with aromatic regions on microplastic surfaces through π–π stacking and hydrophobic associations [41–43], competing for adsorption sites (Freundlich model, $R^2 > 0.95$; Figure S4). Together, these processes destabilized surface binding, resulting in a 3.2–6.4-fold enhancement of EDPB release in intestinal fluid relative to the corresponding water controls for each polymer, with the strongest effect observed at 37 °C. These findings underscore that hydrophobic interactions, π–π stacking, and micelle-induced solubilization collectively dominate the desorption of FLCMs within gastrointestinal environments, thereby controlling their bioaccessibility and

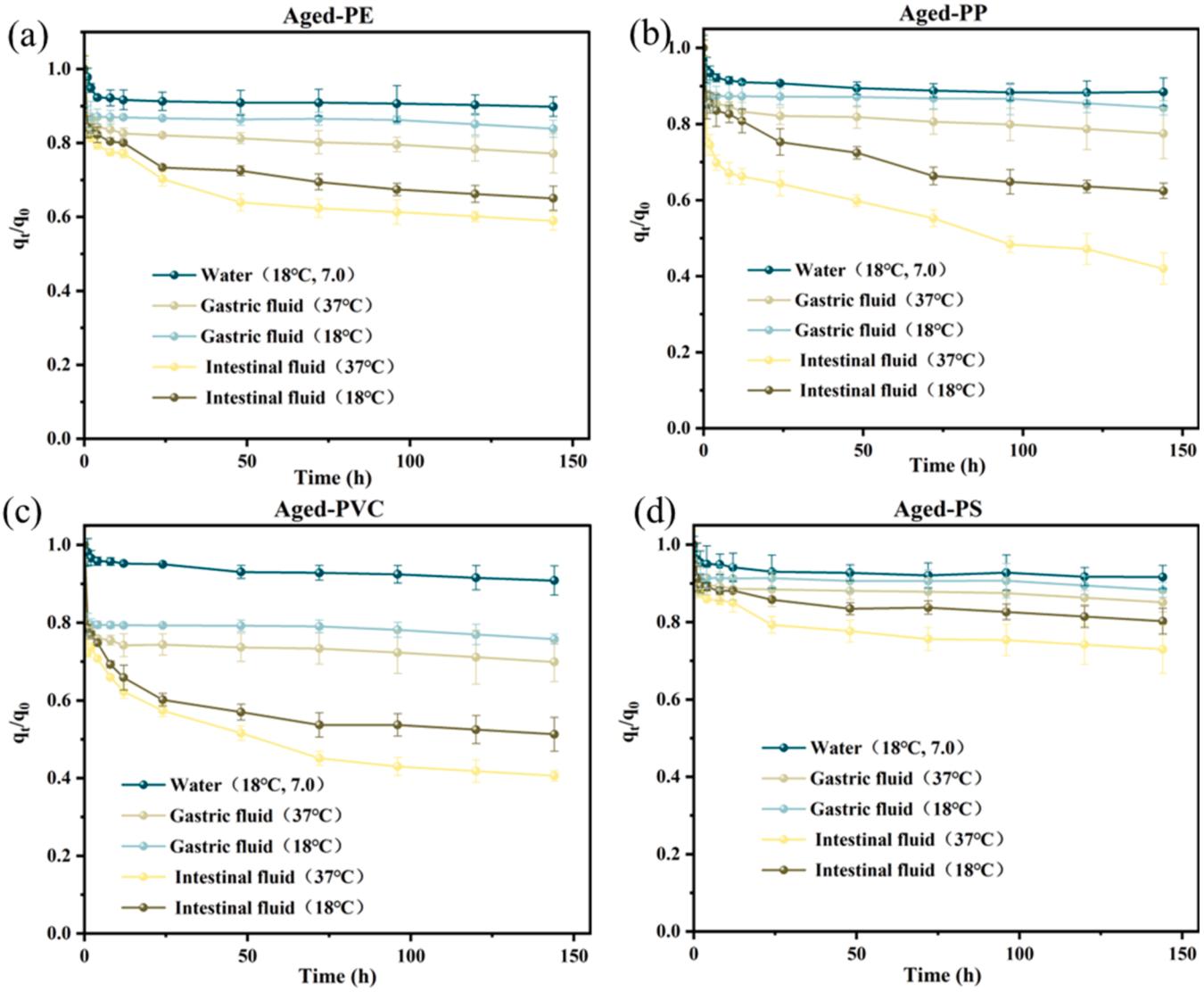


Fig. 2. Desorption kinetics of EDPB from aged microplastics in water, simulated gastric and intestinal fluids at varying temperatures. (a) aged-PE; (b) aged-PP; (c) aged-PVC; and (d) aged-PS. Error bars represent the standard deviation values (n = 3).

potential for trophic transfer.

3.2.2. Bioaccessibility and desorption dynamics in simulated gastrointestinal systems

Simulated digestion experiments revealed that substantial fractions of EDPB bound to aged microplastics became bioaccessible during sequential gastric (2 h) and intestinal (4 h) exposure. Overall desorption of EDPB ranged from 29.4–52.8% across various aged microplastics and temperatures (Fig. 3a), with significantly higher release under warm-blooded conditions ($p < 0.05$). The high desorption observed in intestinal fluid (up to 52.8%) indicates a markedly enhanced bioaccessibility of EDPB when carried by aged microplastics. However, it should be noted that bioaccessibility represents a conservative upper limit for bioavailability; actual systemic uptake and internal dose would further depend on epithelial transport and metabolic processes. Prolonged exposure (gastric 36 h; intestinal 84 h) further increased cumulative desorption to 67.7–94.2% (Fig. 3b), demonstrating temperature- and duration-dependent enhancement. These results indicate that both higher body temperature and extended digestion favor pollutant mobilization, implying greater exposure potential for warm-blooded organisms. The observed desorption behavior aligns with established frameworks for hydrophobic organic contaminants (HOCs) (Table S8). While highly hydrophobic compounds (e.g., PAHs, PCBs) typically rely on micellar solubilization for intestinal release, EDPB exhibited pronounced desorption consistent with a dual mechanism: bile salt-mediated solubilization and aging-induced surface modifications.

Desorption hysteresis differed markedly among polymer types. The Hysteresis Index (HI) decreased in the order PVC > PS > PE > PP (Table S7 and Figure S5), with stronger hysteresis in glassy polymers (PVC, PS) due to restricted intramatrix diffusion [44–46]. Hysteresis was more pronounced in gastric than intestinal fluid, consistent with the lower bioaccessibility observed under acidic conditions. In intestinal fluids at 37 °C, hysteresis largely disappeared, likely because elevated temperature and surfactant activity accelerated EDPB desorption kinetics. At intestinal pH, deprotonation of surface carboxyl groups may enhance negative surface charge, potentially increasing electrostatic repulsion and facilitating the detachment of EDPB-associated micelles. Additionally, the reduction of hysteresis suggests that digestive conditions may induce partial matrix swelling or structural relaxation, thereby opening previously restricted diffusion pathways and promoting the release of EDPB sequestered within microporous domains. Isotherm analysis supported a microporous-filling behavior, where pore swelling at high EDPB concentrations enhanced retention in glassy matrices. Therefore, adsorption affinity and mechanical rigidity jointly governed the desorption lag and overall bioaccessibility.

Environmental parameters strongly modulated EDPB release.

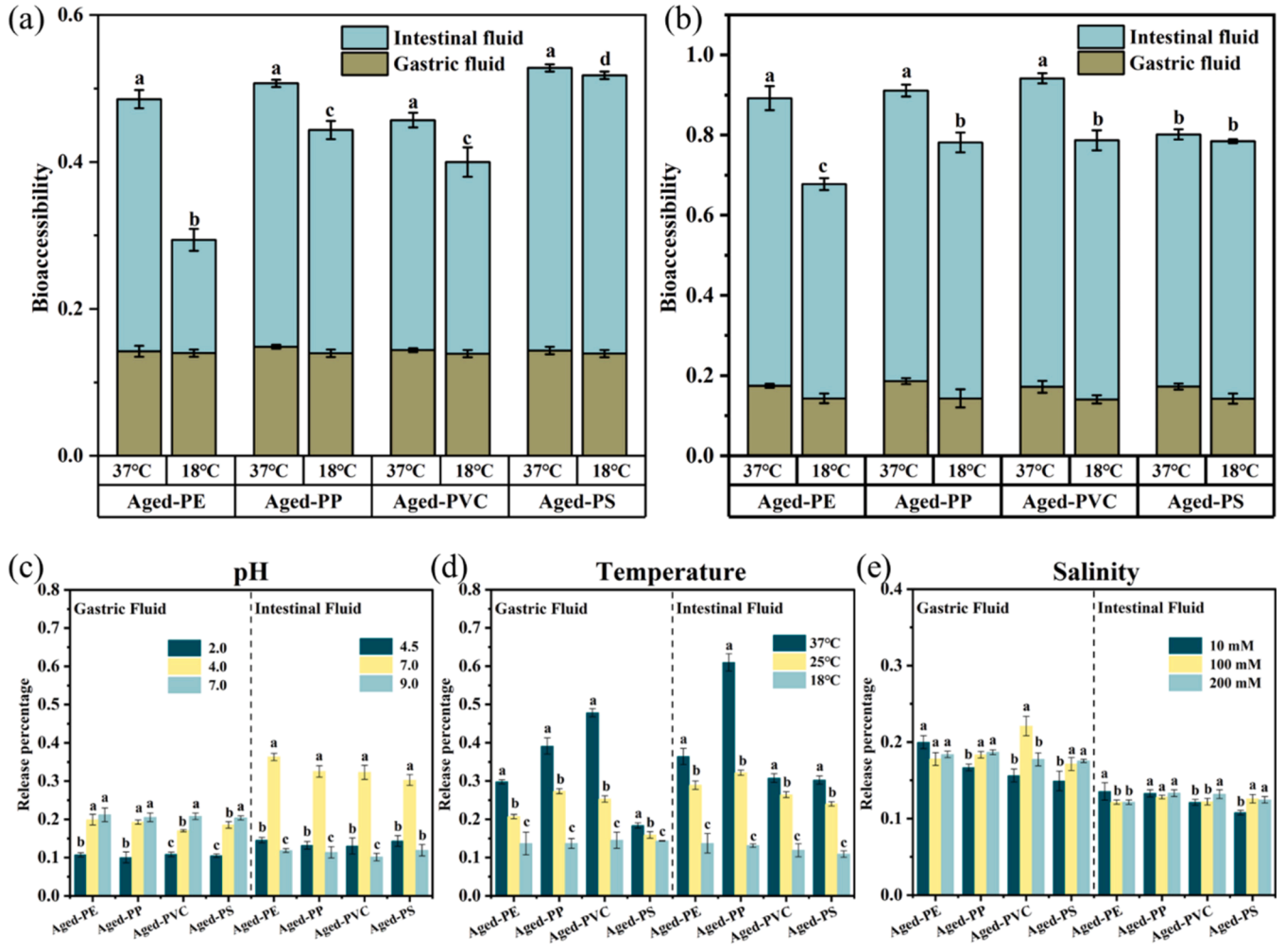


Fig. 3. Bioaccessibility and desorption of EDPB from aged microplastics under simulated gastrointestinal and physiological conditions. (a) Release in gastric fluid for 2 h followed by intestinal fluid for 4 h; (b) Release in gastric fluid for 36 h followed by intestinal fluid for 84 h; (c) pH-dependent desorption in gastric and intestinal fluids; (d) Temperature effects on desorption kinetics; (e) Salinity effects on EDPB release. Error bars represent duplicate variances. Different letters indicate significant differences ($p < 0.01$). Unless otherwise specified, experimental conditions were fixed at a microplastic dose of 0.064 g, salinity of 100 mM NaCl, and standard fluid conditions (gastric: 37 °C, pH 2.0; intestinal: 18 °C, pH 7.0).

Desorption capacity followed the order PVC > PP > PE > PS (Table S2), inversely correlated with sorption affinity. Increasing pH reduced electrostatic attraction and hydrophobic binding above the polymer isoelectric points (pH > 4), promoting desorption ($p < 0.05$), whereas excessive alkalinity (pH 9) induced surface shrinkage [47,48] that hindered release (Fig. 3c). Elevated temperature (18 *vs.* 37 °C) enhanced the fast-desorption rate constant (K_{fast}) by 7–201% (Fig. 3d), confirming an endothermic ($\Delta H_{(D)} > 0$), entropy-driven ($\Delta S_{(D)} > 0$), spontaneous process ($\Delta G_{(D)} < 0$) (Table S7). Pepsin catalysis further amplified desorption in gastric fluid, yielding 2.5–3.1-fold higher release than enzyme-free controls, whereas π–π interaction-dominated adsorption on PS [49] showed minimal temperature response. Salinity exhibited medium-specific effects on desorption. High ionic strength (200 mM NaCl) suppressed desorption in gastric fluid (−24.6%) but enhanced it in intestinal fluid (+8.1%) (Fig. 3e). This contrasting behavior reflects the competition between salting-out effects and bile-salt-mediated solubilization [33,50].

These findings demonstrate that the desorption and bioaccessibility of FLCMs from aged microplastics are governed by the coupled influences of polymer microstructure, digestive chemistry, and environmental factors. Variations in polymer rigidity and surface functionality define the strength of contaminant binding, while temperature, pH, enzymatic activity, and salinity dynamically modulate interfacial interactions within gastrointestinal environments. The combined action of these parameters determines the extent to which FLCMs are remobilized and become bioaccessible, ultimately shaping their environmental fate and ecological risk potential.

3.3. Biological responses to aged microplastic-associated EDPB

While desorption kinetics define the physical bioaccessibility of FLCMs, their toxicological implications depend on how the released fraction interacts with biological systems at the cellular level. Released EDPB can permeate intestinal epithelial barriers and potentially induce cellular stress responses. To elucidate these downstream effects, cytotoxicity and transcriptomic responses of Caco-2 cells [51] were investigated following exposure to EDPB at concentrations comparable to those measured in simulated gastrointestinal fluids. This design ensures that in vitro exposures reflect the bioaccessible fraction released under physiological conditions.

3.3.1. Concentration-dependent cytotoxicity and mechanisms of EDPB in Caco-2 cells

Microscopic observations showed marked morphological changes in Caco-2 cells after 24 h EDPB exposure, with cells rounding and shrinking from a typical epithelial morphology (Figure S6). The 24 h in vitro cytotoxicity assay yielded an IC_{50} of 80540 μg L^{-1} (Figure S7), comparable in magnitude to values reported for representative PCB congeners. This exposure level is 2–3 orders of magnitude higher than LCM concentrations currently reported in human serum (3.16–276 μg L^{-1}) [52]. Nevertheless, the results highlight the potential risks of chronic low-dose exposure, particularly in light of the environmental persistence and

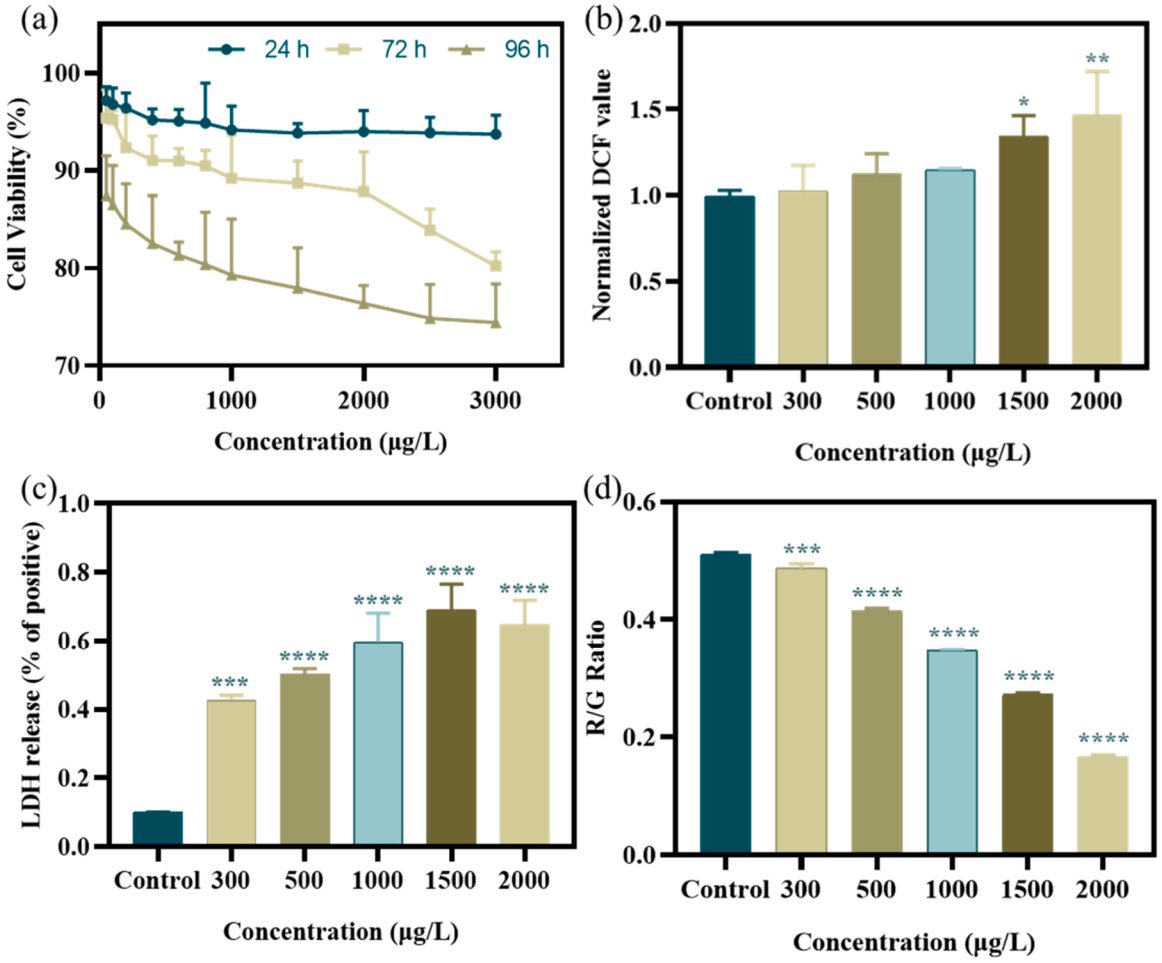


Fig. 4. Cytotoxic effects of EDPB exposure on Caco-2 intestinal epithelial cells. (a) Concentration-dependent effects on cell viability assessed by CCK-8 assay; (b) intracellular reactive oxygen species generation measured by DCFH-DA fluorescence; (c) lactate dehydrogenase release as an indicator of membrane integrity; (d) mitochondrial membrane potential evaluated using JC-1 staining. Data are presented as mean ± SD (n = 6) (*$p < 0.05$; **$p < 0.01$; ***$p < 0.001$; ****$p < 0.0001$).

cumulative toxicity of FLCMs. CCK-8 assays revealed a significant time- and concentration-dependent gradient in EDPB toxicity. Cell viability decreased from 96.4% at 24 h to 87.4% after 96 h of exposure to 50 μg L^{-1} ($p = 0.0075$, Fig. 4a), while exposure to 2000 μg L^{-1} dramatically reduced viability to 74.3% after 96 h (*vs.* 96.1% at 24 h, $p < 0.0001$), indicating that prolonged high-dose exposure exacerbates cytotoxic damage. LDH leakage assays confirmed that exposure to greater than 300 μg L^{-1} for 72 h caused significant membrane damage ($p = 0.0001$, Fig. 4c). DCFH-DA probe analysis revealed that exposure to concentrations greater than 1500 μg L^{-1} triggered excessive reactive oxygen species (ROS) production (Fig. 4b), while exposure to 300 μg L^{-1} significantly disrupted mitochondrial membrane potential ($p = 0.0001$, Fig. 4d).

The toxic effects of EDPB showed a clear concentration-dependent pattern. Exposure to 50 μg L^{-1} for 96 h reduced cell viability to 87.4% ($p = 0.0075$). At higher concentrations, 300 μg L^{-1} caused mitochondrial membrane potential collapse, 1500 μg L^{-1} induced excessive ROS production, and 2000 μg L^{-1} further decreased cell viability to 74.3% ($p < 0.0001$). Integration of these endpoints demonstrates a concentration-dependent cascade of cellular injury. Sublethal exposure initially disrupted mitochondrial membrane potential, leading to excessive ROS production and oxidative stress, which subsequently impaired membrane integrity and cell viability. This mechanistic progression from mitochondrial dysfunction to oxidative damage, and eventual cell death highlights energy metabolism and redox imbalance as central pathways in EDPB cytotoxicity.

3.3.2. *Transcriptomic profiling*

To elucidate the molecular mechanisms underlying the observed cytotoxicity, oxidative stress, and membrane injury induced by EDPB, transcriptomic sequencing was conducted to analyze the global molecular regulatory response and key signaling pathways mediated by EDPB in Caco-2 cells. RNA sequencing (RNA-seq; n = 6) yielded high-quality datasets, generating a total of 40.19 Gb of clean reads, with Q30 scores exceeding 96.7%, confirming high sequencing accuracy and data reliability. Sample correlation heatmaps further displayed strong intra- and inter-group consistency (Pearson correlation coefficients ≥ 0.943 within groups and ≥ 0.947 between groups; Fig. 5a), ensuring the robustness of the dataset for downstream analysis at the transcriptional level. In total, 545 and 414 uniquely expressed genes were identified in the control and treated groups, respectively, along with 12,394 co-expressed genes (Fig. 5b).

The transcriptional profile revealed a predominance of down-regulated genes following EDPB exposure, suggesting a global inhibitory cellular response. Differential expression analysis identified 1448 EDPB-responsive genes, i.e., differentially expressed genes (DEGs), including

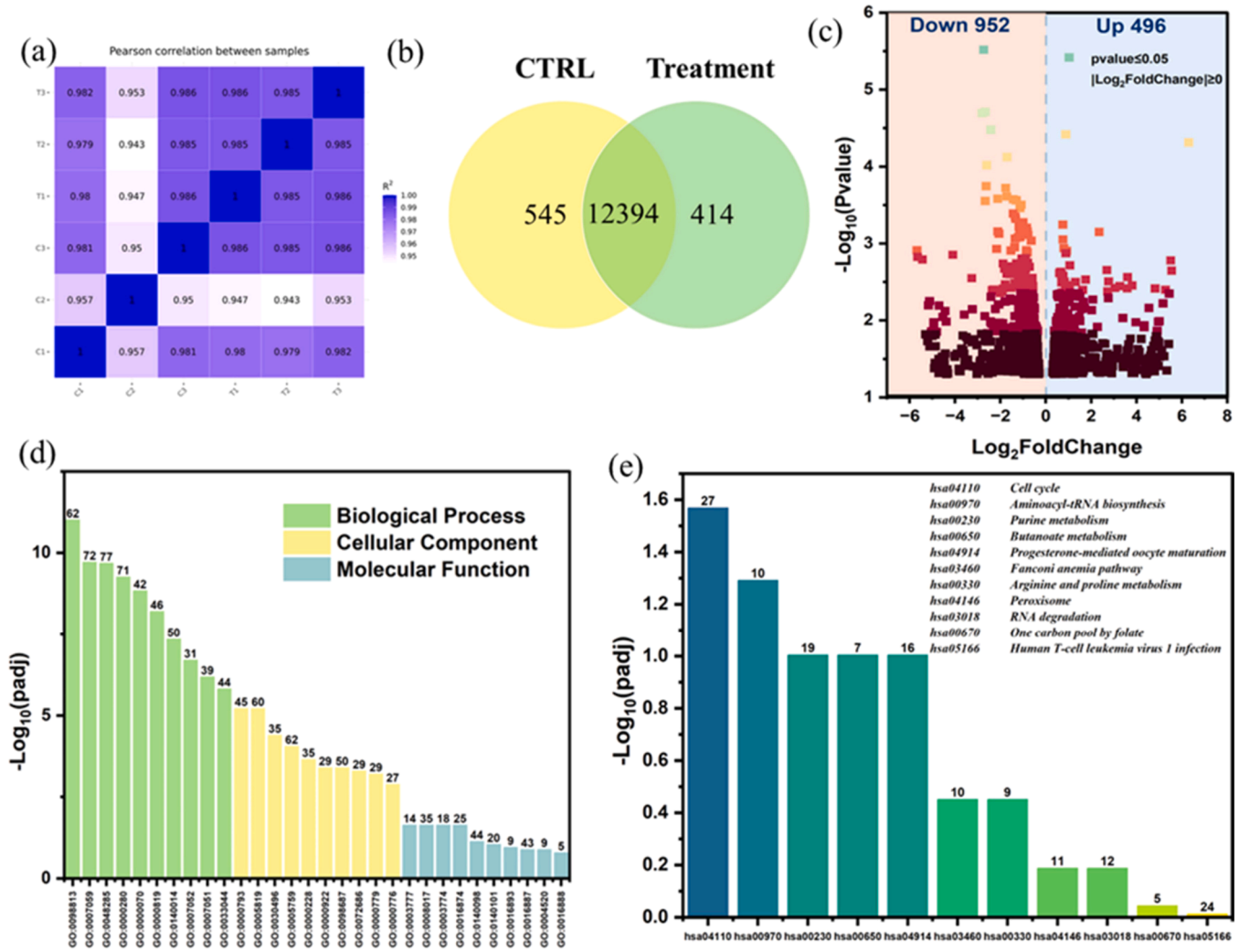


Fig. 5. Transcriptomic profiling reveals systemic alterations in gene expression patterns following EDPB exposure. (a) Inter-sample correlation analysis demonstrating treatment-induced transcriptional changes; (b) Venn diagram quantifying overlapping and unique co-expressed genes between treatment and control groups; (c) Volcano plot of differentially expressed genes ($p < 0.05$, $|log2FC| > 1$); (d) GO enrichment analysis showing significantly affected biological processes (color-coded by functional category); (e) KEGG pathway enrichment histogram revealing perturbed metabolic and signaling pathways.

952 downregulated (65.75%) and 496 upregulated (34.25%) transcripts (Fig. 5c). Notably, the top five downregulated genes (*HIST2H4B, ACSM3, EHF, DLC1, GPRIN3*) were significantly associated with epigenetic modifications and metabolic homeostasis, while the top five upregulated genes (*RN7SL2, TMEM191A, KRT34, S1PR2, GAGE13*) were primarily linked to inflammatory activation and RNA metabolic dysregulation. GO enrichment analysis (Fig. 5d) ($padj < 0.05$) revealed that DEGs were enriched in chromosome segregation ($n = 72$), nuclear division ($n = 71$), and microtubule-binding functions ($n = 35$), reflecting disrupted cell cycle regulation and mitotic apparatus integrity. KEGG pathway analysis (Fig. 5e) further indicated that EDPB perturbs genomic stability and cell fate balance by impairing the Fanconi anemia pathway (DNA damage repair), purine/butyrate metabolism (energy homeostasis), and RNA degradation pathway (genetic information fidelity).

Overall, these transcriptomic signatures (Fig. 5) demonstrate that EDPB acts as a potent disruptor of genomic maintenance and metabolic homeostasis, shifting the cell fate toward growth arrest and functional decline.

3.3.3. *Mechanisms of toxicity*

Fig. 6 illustrates a hierarchical toxicological framework identifying EDPB as a metabolic disruptor. Integrated transcriptomic and biochemical evidence indicates that mitochondrial dysfunction–driven oxidative stress is the primary toxicological mechanism, while cell cycle dysregulation and genomic instability occurred as downstream consequences. The process begins with impaired energy-producing organelles, triggering a cascade of oxidative damage that culminates in the genomic instability (Fig. 6a) and cell cycle arrest (Fig. 6b).

At the metabolic level, EDPB markedly suppressed mitochondrial energy production. Key tricarboxylic acid (TCA) cycle enzymes, including *DLAT* (FC = 0.63) and *SDHB* (FC = 0.82), were significantly downregulated, indicating impaired carbon flux and intermediate metabolite accumulation. Consistently, reduced transcript levels of electron transport chain components (*NDUFV3*, FC = 0.58; *COX7A2*, FC = 0.97; *ATP5F1A*, FC = 0.63) confirmed the inhibition of oxidative phosphorylation [53]. Concurrent dysregulation of purine (*IMPDH2*, FC = 0.66) and butyric acid metabolism (*ACADS*, FC = 0.83) further constrained compensatory energy pathways, establishing a state of bioenergetic deficiency and redox imbalance [54].

This metabolic collapse triggered oxidative stress and membrane destabilization. Suppression of peroxisomal biogenesis and β-oxidation genes (*Pex1*, FC = 0.35; *SCPX*, FC = 0.66) likely promoted lipotoxicity, while inhibited *PPAR-γ* signaling weakened mitochondrial antioxidant defenses (FC = 0.88). Consequently, intracellular ROS levels increased 1.98-fold, resulting extensive lipid peroxidation and a 6.7-fold elevation in LDH leakage [55,56]. Consistent with other LCM-like pollutants, *PPAR-γ* antagonism serves as a critical regulatory node linking mitochondrial dysfunction to oxidative stress, rather than acting as independently [57].

Downstream effects of this metabolic-oxidative axis included disrupted cell cycle progression and genomic maintenance. Genes governing chromosome segregation and spindle assembly were broadly suppressed. Downregulation of *Cyclins* and *CDKs* impaired complex activation, resulting in G_1/S phase arrest, while reduced DNA replication initiation factors (*MCM2–7*, FC = 0.71–0.88) compromised replication competence [58,59]. Additionally, *CDC20* inhibition (FC = 0.28) impaired APC/C function, and suppressed DNA repair genes (*RAD21*, FC = 0.69; *DDX11*, FC = 0.84) reduced genome stability. *PLK1* downregulation (FC = 0.24) further disrupted spindle organization, exacerbating chromosomal mis-segregation [60].

The toxicological response followed a clear, hierarchical progression: at 50 μg L^{-1}, EDPB primarily disrupted mitochondrial metabolic pathways, signaling early bioenergetic stress. Moderate exposure (300 μg L^{-1}) amplified cell cycle inhibition, while high concentrations (2000 μg L^{-1}) triggered pronounced oxidative damage and apoptosis, as confirmed by caspase-9/-3 activation [61]. This concentration-dependent mode of action resembles patterns observed for established persistent organic pollutants [62–64], suggesting that EDPB engages conserved metabolic and redox-sensitive pathways that may contribute to epithelial cell stress.

Notably, these effects were evaluated using dissolved EDPB to specifically isolate the hazards of the bioaccessible fraction released from microplastics. This model establishes a direct mechanistic linkage between desorbed pollutants and subsequent cellular responses. While the EDPB released via the 'vector effect' is shown here to sufficiently trigger mitochondrial dysfunction, representing a conservative risk estimation. In a real-world scenario, microplastic particles may further exacerbate toxicity through physical irritation or localized 'hotspot' release upon cell-particle contact. Consequently, future studies incorporating MP-EDPB complexes are essential to resolve these potential synergistic effects.

4. Conclusion

In this study, the molecular mechanisms underlying the adsorption–desorption behavior of EDPB on aged microplastics under simulated gastrointestinal conditions and their induction of intestinal epithelial cell (Caco-2) toxicity were systematically elucidated. UV aging, a key environmental weathering process driven by solar irradiation during prolonged environmental exposure (e.g., floating in surface waters or stranded on beaches for months to years), significantly enhanced the adsorption capacity of microplastics for EDPB. The aging process induced three characteristic modifications in microplastics: surface roughening, particle size reduction, and generation of oxygen-containing functional groups such as hydroxyl and carboxyl groups, consistent with the chemical features of naturally weathered marine microplastics. These physicochemical transformations promoted the formation of persistent composite pollutant carriers capable of accumulating and transferring through aquatic food webs. Our findings highlight that UV-aging of microplastics increases the bioaccessibility of sorbed FLCMs in the human gastrointestinal tract, thereby potentially increasing their toxicological risk, although further studies are needed to quantify the exact bioavailability. Simulated gastrointestinal experiment demonstrated that fluidic conditions efficiently remobilized adsorbed EDPB, with desorption peaks (F_{fast}) observed at 37 °C, leading to enhanced bioaccessibility and potential intestinal exposure. Mechanistic investigations revealed that EDPB initiates a toxicological cascade originating from metabolic and redox disruption. Specifically, EDPB functions as a primary metabolic insult by inhibiting *PPAR-γ* signaling and impairing mitochondrial bioenergetics (TCA cycle and electron transport chain). This metabolic collapse induces oxidative stress that drives downstream genomic instability, characterized by the suppression of *Cyc*/CDK complexes, APC/C function, and DNA repair pathways, culminating in caspase-dependent apoptosis.

The ecological implications of these findings extend beyond human intestinal epithelium, but also potentially threaten ecosystem function (microbial communities) and aquatic organisms through food-web transmission. The environmental persistence and mobility of microplastic-EDPB complexes amplify their exposure potential, placing non-target organisms (e.g., zooplankton, gut microbiota) at risk of irreversible oxidative stress-and lipotoxicity-induced damage. Future research should prioritize the cumulative effects of chronic low-dose exposure and interactive toxicity with co-pollutants, alongside establishing toxicity thresholds and risk assessment frameworks specific to microplastic-LCM contamination.

Environmental implication

Fluorinated liquid crystal monomers (FLCMs), whose environmental behavior is influenced by ubiquitous microplastics, represent emerging organic contaminants of concern with increasing environmental relevance. This study shows that environmentally aged microplastics serve

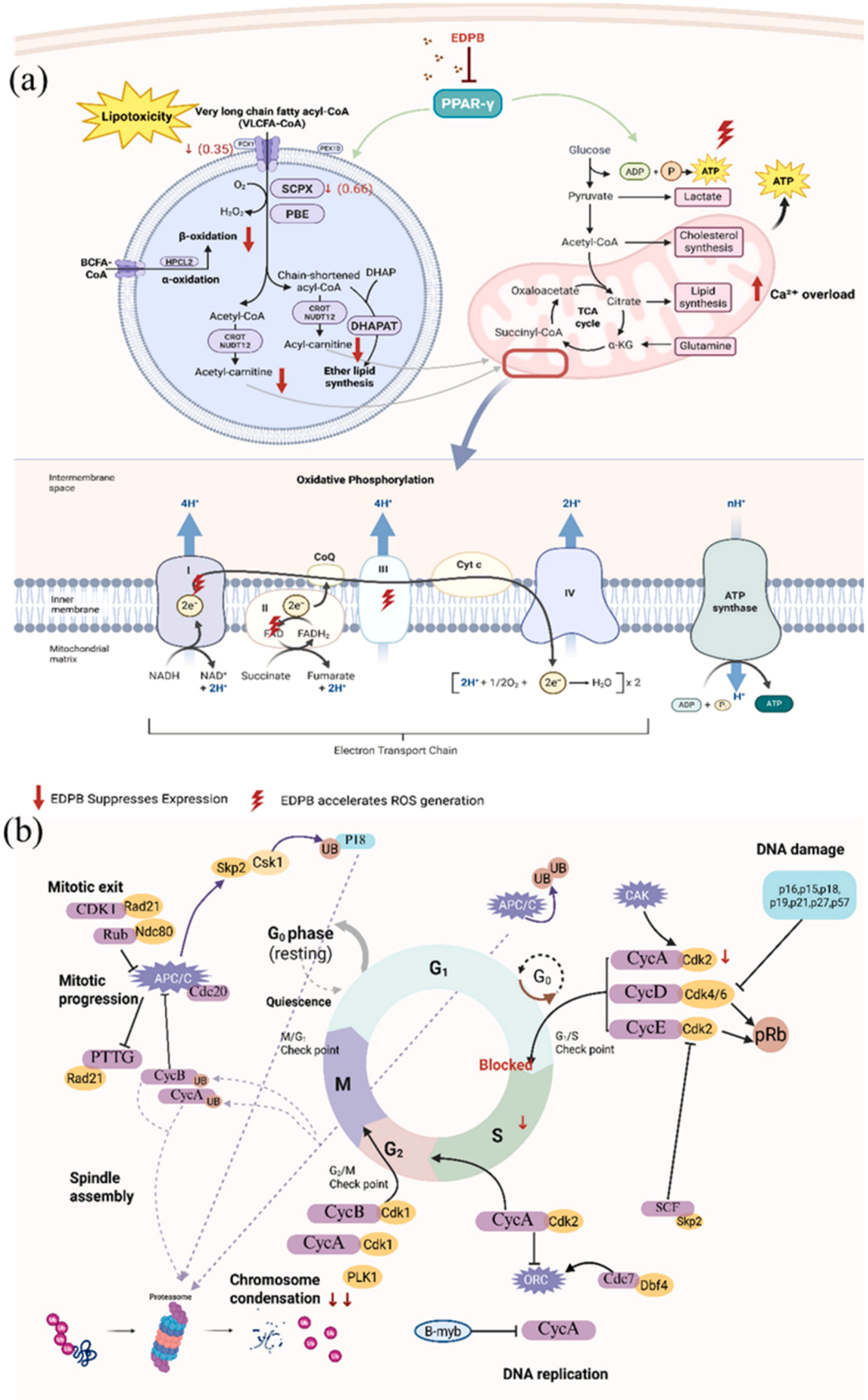


Fig. 6. Impact of EDPB exposure on Caco-2 cells. (a) Impairment of peroxisomal and mitochondrial function: suppression of *DLAT*, *SDHB*, *Pex1*, and *SCPX*, together with *PPAR-γ* inhibition, led to TCA cycle imbalance, excessive ROS generation, calcium overload, and caspase-dependent apoptosis. (b) Disruption of cell cycle regulation: downregulation of *Cycs*, *CDK*, *CDC20*, and *RAD21* inhibited the Cyc/CDK complex and APC/C function, causing G_1/S-phase arrest and genomic instability. In summary, EDPB disrupts intestinal epithelial integrity through a *PPAR-γ*-mediated mitochondrial-to-nuclear stress axis.

as efficient sinks and sources for FLCMs, enhancing their accumulation and bioaccessible release under biologically relevant conditions. The remobilization of microplastic-associated FLCMs increases potential biological exposure, with oxidative stress–mediated toxicity observed in intestinal epithelial cells. By linking environmental aging, bioaccessibility, and toxicological responses, this work provides critical insight into FLCM behavior and supports improved risk assessment of microplastic-associated emerging contaminants.

CRediT authorship contribution statement

Mui-Choo Jong: Writing – review & editing, Supervision, Project administration, Funding acquisition. **Season Si Chen:** Writing – review & editing, Supervision, Project administration, Methodology, Funding acquisition. **Apple Pui-Yi Chui:** Writing – review & editing, Writing – original draft. **Sanjeeb Mohapatra:** Writing – review & editing, Writing – original draft. **Rui Yang:** Writing – review & editing, Writing – original draft, Investigation, Formal analysis, Data curation, Conceptualization.

Declaration of Competing Interest

The authors declare that they have no known competing financial interests or personal relationships that could have appeared to influence the work reported in this paper.

Acknowledgements

This work is implemented through the support of Shenzhen Science and Technology Innovation Commission (JCYJ20230807111605010), the Shenzhen Science and Technology Program (ZDSYS20220606100806014), the Scientific Research Startup Fund of SIGS, Tsinghua University (QD2023001C and QD2023007C), and the Guangdong Higher Education Institutions Innovative Research Team of Urban Water Cycle and Ecological Safety (2023KCXTD053).

Appendix A. Supporting information

Supplementary data associated with this article can be found in the online version at doi:10.1016/j.jhazmat.2026.141802.

Data availability

All experimental data, including tables, figures, and analysis results, are provided in the manuscript or the Supporting Information uploaded in Attach Files.

References

[1] Liu, Y., Kannan, K., 2024. Concentrations, profiles, and potential sources of liquid crystal monomers in residential indoor dust from the United States. Environ Sci Technol 58, 12400–12408.
[2] Feng, Y., Wu, J., Lao, W., Ye, W., Guo, D., Wang, Z., Wu, X., Lai, R.W.S., 2025. Micro- and nanoplastic-mediated phototransformation and bioaccessibility of fluorinated liquid crystal monomer in aquatic environments. Environ Sci Nano 12, 248–261.
[3] Feng, J.J., Sun, X.F., Zeng, E.Y., 2022. Emissions of liquid crystal monomers from obsolete smartphone screens in indoor settings: characteristics and human exposure risk. Environ Sci Technol 56, 8053–8060.
[4] Liang, X.X., Xie, R.M., Zhu, C.Y., Chen, H., Shen, M.J., Li, Q., Du, B.B., Luo, D., Zeng, L.X., 2021. Comprehensive identification of liquid crystal monomers-biphenyls, cyanobiphenyls, fluorinated biphenyls, and their analogues-in waste LCD panels and the first estimate of their global release into the environment. Environ Sci Technol 55, 12424–12436.
[5] Mohapatra, S., Jong, M.C., Mukherji, S., van Lier, J.B., Spanjers, H., 2025. Liquid crystal monomers (LCMs) of emerging concern: recent progress and challenges in wastewater treatment. Curr Pollut Rep 11, 48.
[6] Zhu, M.S., Shen, M.J., Liang, X.X., Chen, H., Zhu, C.Y., Du, B.B., Luo, D., Lan, S.Y., Feng, Z.Q., Zeng, L.X., 2021. Identification of environmental liquid-crystal monomers: a class of new persistent organic pollutants-fluorinated biphenyls and analogues-emitted from e-waste dismantling. Environ Sci Technol 55, 5984–5992.
[7] Su, H.J., Ren, K.F., Li, R.R., Li, J.H., Gao, Z.Q., Hu, G.J., Fu, P.Q., Su, G.Y., 2022. Suspect screening of liquid crystal monomers (LCMs) in sediment using an established database covering 1173 LCMs. Environ Sci Technol 56, 8061–8070.
[8] Wang, Y., Jin, Q., Lin, H., Xu, X., Leung, K.M.Y., Kannan, K., He, Y., 2024. A review of liquid crystal monomers (LCMs) as emerging contaminants: Environmental occurrences, emissions, exposure routes and toxicity. J Hazard Mater 480, 135894.
[9] Yang, R., Xu, X., Wang, X., Niu, Y., Du, J., Li, H., Chen, X., Li, G., Shao, B., 2024. Fluorinated Liquid-Crystal Monomers in Serum from the General Population and Their Impact on Human Health. Environ Sci Technol 58, 15949–15959.
[10] Rynek, R., Tekman, M.B., Rummel, C., Bergmann, M., Wagner, S., Jahnke, A., Reemtsma, T., 2024. Hotspots of Floating Plastic Particles across the North Pacific Ocean. Environ Sci Technol 58, 4302–4313.
[11] Wu, P.F., Tang, Y.Y., Dang, M., Wang, S.Q., Jin, H.B., Liu, Y.S., Jing, H., Zheng, C. M., Yi, S.P., Cai, Z.W., 2020. Spatial-temporal distribution of microplastics in surface water and sediments of Maozhou River within Guangdong-Hong Kong-Macao Greater Bay Area. Sci Total Environ 717, 135187.
[12] Zhou, Q., Zhang, H., Fu, C., Zhou, Y., Dai, Z., Li, Y., Tu, C., Luo, Y., 2018. The distribution and morphology of microplastics in coastal soils adjacent to the Bohai Sea and the Yellow Sea. Geoderma 322, 201–208.
[13] Chai, B., Wei, Q., She, Y., Lu, G., Dang, Z., Yin, H., 2020. Soil microplastic pollution in an e-waste dismantling zone of China. Waste Manag (Oxf) 118, 291–301.
[14] Liu, X.M., Shi, H.H., Xie, B., Dionysiou, D.D., Zhao, Y.P., 2019. Microplastics as Both a Sink and a Source of Bisphenol A in the Marine Environment. Environ Sci Technol 53, 10188–10196.
[15] Li, X., Kong, Y., Juhasz, A.L., Zhou, P., Zhang, Q., Cui, X., 2023. Effect of Microplastic Types on the In Vivo Bioavailability of Polychlorinated Biphenyls. Environ Sci Technol 57, 12838–12846.
[16] Hou, G., Zhao, X., Zhao, T., Wu, X., Pu, S., Tang, Z., Wu, F., 2023. The adsorption of PAHs on microplastics and desorption in the simulated human digestive system. Chem Eng J 473, 145157.
[17] Chen, X., Yu, X., Zhang, L., Zhao, W., Sui, Q., 2024. Organic pollutants adsorbed on microplastics: Potential indicators for source appointment of microplastics. J Hazard Mater 465, 133225.
[18] Wang, Q., Gao, Y., Tang, X., Yang, Z., Tang, L., Luo, G., Liu, C., Tong, H., 2025. How aging microplastics influence heavy metal environmental fate and bioavailability: A systematic review. Environ Res 271, 121128.
[19] Dayal, L., Raj, D., Kumari, P., Sinha, S., 2024. Abundance of Microplastics in Marine and Freshwater Ecosystem and it's Impact on Biotic and Abiotic Components. Water Air Soil Pollut 235, 416.
[20] Parolini, M., Stucchi, M., Ambrosini, R., Romano, A., 2023. A global perspective on microplastic bioaccumulation in marine organisms. Ecol Indic 149, 110179.
[21] Bakir, A., Rowland, S.J., Thompson, R.C., 2014. Enhanced desorption of persistent organic pollutants from microplastics under simulated physiological conditions. Environ Pollut 185, 16–23.
[22] Emecheta, E.E., Pfohl, P.M., Wohlleben, W., Haase, A., Roloff, A., 2024. Desorption of Polycyclic Aromatic Hydrocarbons from Microplastics in Human Gastrointestinal Fluid Simulants—Implications for Exposure Assessment. ACS Omega 9, 24281–24290.
[23] Nor, N.H.M., Koelmans, A.A., 2019. Transfer of PCBs from Microplastics under Simulated Gut Fluid Conditions Is Biphasic and Reversible. Environ Sci Technol 53, 1874–1883.
[24] Masset, T., Ferrari, B.J.D., Dudefoi, W., Schirmer, K., Bergmann, A., Vermeirssen, E., Grandjean, D., Harris, L.C., Breider, F., 2022. Bioaccessibility of Organic Compounds Associated with Tire Particles Using a Fish In Vitro Digestive Model: Solubilization Kinetics and Effects of Food Coingestion. Environ Sci Technol 56, 15607–15616.
[25] Prajapati, A., Narayan Vaidya, A., Kumar, A.R., 2022. Microplastic properties and their interaction with hydrophobic organic contaminants: a review. Environ Sci Pollut Res 29, 49490–49512.
[26] Wang, T., Wang, L., Chen, Q., Kalogerakis, N., Ji, R., Ma, Y., 2020. Interactions between microplastics and organic pollutants: Effects on toxicity, bioaccumulation, degradation, and transport. Sci Total Environ 748, 142427.
[27] Cox, K.D., Covernton, G.A., Davies, H.L., Dower, J.F., Juanes, F., Dudas, S.E., 2019. Human Consumption of Microplastics. Environ Sci Technol 53, 7068–7074.
[28] Yang, R., Wang, X., Gao, Q., Sang, C., Zhao, Y., Niu, Y., Shao, B., 2023. Dietary Exposure and Health Risk of the Emerging Contaminant Fluorinated Liquid-Crystal Monomers. Environ Sci Technol 57, 6309–6319.
[29] He, S., Wu, E., Shen, M., Ji, H., Zeng, L., Zhu, M., 2023. Role of Substituents in the Removal of Emerging Fluorinated Liquid Crystal Monomer Pollutants under the UV/Peroxydisulfate Treatment. ACS ES&T Eng 3, 651–660.
[30] Geyer, R., Jambeck, J.R., Law, K.L., 2017. Production, use, and fate of all plastics ever made. Sci Adv 3, 1700782.
[31] Binda, G., Kalčíková, G., Allan, I.J., Hurley, R., Rødland, E., Spanu, D., Nizzetto, L., 2024. Microplastic aging processes: Environmental relevance and analytical implications. TrAC Trends Anal Chem 172, 117566.
[32] Tang, S., Sun, P.P., Qu, G.J., Tian, Y., Liu, J.L., Pervez, M.N., Li, X.Y., Cao, C.J., Zhao, Y.P., 2023. Photo-aged non-biodegradable and biodegradable mulching film microplastics alter the interfacial behaviors between agricultural soil and inorganic arsenic. J Hazard Mater 455, 131552.
[33] Liu, P., Wu, X.W., Liu, H.Y., Wang, H.Y., Lu, K., Gao, S.X., 2020. Desorption of pharmaceuticals from pristine and aged polystyrene microplastics under simulated gastrointestinal conditions. J Hazard Mater 392, 122346.
[34] Wagstaff, A., Petrie, B., 2022. Enhanced desorption of fluoxetine from polyethylene terephthalate microplastics in gastric fluid and sea water. Environ Chem Lett 20, 975–982.

[35] Zhao, Q.Z., Zou, Y.Y., Huang, C.H., Lan, P., Zheng, J., Ou, S.Y., 2017. Formation of a Hydroxymethylfurfural-Cysteine Adduct and Its Absorption and Cytotoxicity in Caco-2 Cells. J Agric Food Chem 65, 9903–9909.
[36] Wu, J., Bian, C., Yang, X., Su, G., 2025. CytoToxLCM: A Software to Predict Cytotoxicity of Emerging Contaminant Liquid Crystal Monomers. Environ Sci Technol 59, 7028–7038.
[37] Ren, Z.F., Gui, X.Y., Wei, Y.Q., Chen, X., Xu, X.Y., Zhao, L., Qiu, H., Cao, X.D., 2021. Chemical and photo-initiated aging enhances transport risk of microplastics in saturated soils: Key factors, mechanisms, and modeling. Water Res 202, 117407.
[38] Costa, T.B.O., Santana, G.B., Silva, E.M., Conceicao, K.G.A., Diaz, G.Z., Melo, D.Q., Franca, A.M.M., Do Nascimento, R.F., Oliveira, A.G., Santiago-Aguiar, R.S., Campos, O.S., Vidal, C.B., 2024. Impact of UV-B Photoaging on Chlorpyrifos Adsorption by PET Microplastics: Insights from Experimental and DFT Analysis. ACS Omega 9, 46439–46446.
[39] Fournier, E., Etienne-Mesmin, L., Grootaert, C., Jelsbak, L., Syberg, K., Blanquet-Diot, S., Mercier-Bonin, M., 2021. Microplastics in the human digestive environment: A focus on the potential and challenges facing in vitro gut model development. J Hazard Mater 415, 125632.
[40] Lujic, T., Mutic, T., Simovic, A., Vasovic, T., Ivanovic, S., Krstic Ristivojevic, M., Jovanovic, V., Velickovic, T.Cirkovic, 2025. Protein Corona Stability and Removal from PET Microplastics: Analytical and Spectroscopic Evaluation in Simulated Intestinal Conditions. Foods 14.
[41] Kumar, Y.B., Kumar, N., Vaikundamani, S., Nagamani, S., Mahanta, H.J., Sastry, G. M., Sastry, G.N., 2023. Analyzing the aromatic-aromatic interactions in proteins: A2ID 2.0. Int J Biol Macromol 253, 127207.
[42] Wang, Z.Y., Zhao, J., Song, L., Mashayekhi, H., Chefetz, B., Xing, B.S., 2011. Adsorption and Desorption of Phenanthrene on Carbon Nanotubes in Simulated Gastrointestinal Fluids. Environ Sci Technol 45, 6018–6024.
[43] Liu, X.L., Ji, R., Shi, Y., Wang, F., Chen, W., 2019. Release of polycyclic aromatic hydrocarbons from biochar fine particles in simulated lung fluids: Implications for bioavailability and risks of airborne aromatics. Sci Total Environ 655, 1159–1168.
[44] Liu, X., Gharasoo, M., Shi, Y., Sigmund, G., Huffer, T., Duan, L., Wang, Y., Ji, R., Hofmann, T., Chen, W., 2020. Key Physicochemical Properties Dictating Gastrointestinal Bioaccessibility of Microplastics-Associated Organic Xenobiotics: Insights from a Deep Learning Approach. Environ Sci Technol 54, 12051–12062.
[45] Fu, L.N., Li, J., Wang, G.Y., Luan, Y.N., Dai, W., 2021. Adsorption behavior of organic pollutants on microplastics. Ecotoxicol Environ Saf 217, 112207.
[46] Wang, F., Shih, K.M., Li, X.Y., 2015. The partition behavior of perfluorooctanesulfonate (PFOS) and perfluorooctanesulfonamide (FOSA) on microplastics. Chemosphere 119, 841–847.
[47] Shan, J., Wang, J., Zhan, J., Liu, L., Wu, F., Wang, X., 2020. Sorption behaviors of crude oil on polyethylene microplastics in seawater and digestive tract under simulated real-world conditions. Chemosphere 257, 127225.
[48] Martin, J., Santos, J.L., Aparicio, I., Alonso, E., 2022. Microplastics and associated emerging contaminants in the environment: Analysis, sorption mechanisms and effects of co-exposure. Trends Environ Anal Chem 35, e00170.
[49] Xie, A., Chen, S., Liang, X., Li, L., Song, Y., Lv, M., Liang, F., Zhou, W., 2025. Influence of microplastic aging on the adsorption and desorption behavior of Ni(II) under various aging conditions. Environ Geochem Health 47, 87.
[50] Fu, L.N., Li, J., Wang, G.Y., Luan, Y.N., Dai, W., 2021. Adsorption behavior of organic pollutants on microplastics. Ecotoxicol Environ Saf 217, 112207.
[51] Peng, M., Vercauteren, M., Grootaert, C., Catarino, A.I., Everaert, G., Rajkovic, A., Janssen, C., Asselman, J., 2024. Bioenergetic effects of pristine and ultraviolet-weathered polydisperse polyethylene terephthalate and polystyrene nanoplastics on human intestinal Caco-2 cells. Sci Total Environ 908, 168267.
[52] Li, Y., Zhang, T., Cheng, Z., Zhang, Q., Yang, M., Zhao, L., Zhang, S., Lu, Y., Sun, H., Wang, L., 2022. Direct evidence on occurrence of emerging liquid crystal monomers in human serum from E-waste dismantling workers: Implication for intake assessment. Environ Int 169, 107535.
[53] Nunes-Nesi, A., Araújo, W.L., Obata, T., Fernie, A.R., 2013. Regulation of the mitochondrial tricarboxylic acid cycle. Curr Opin Plant Biol 16, 335–343.
[54] Olszewski, K., Barsotti, A., Feng, X.-J., Momcilovic, M., Liu, K.G., Kim, J.-I., Morris, K., Lamarque, C., Gaffney, J., Yu, X., Patel, J.P., Rabinowitz, J.D., Shackelford, D.B., Poyurovsky, M.V., 2022. Inhibition of glucose transport synergizes with chemical or genetic disruption of mitochondrial metabolism and suppresses TCA cycle-deficient tumors. Cell Chem Biol 29, 423–435 e410.
[55] Gardner, B.M., Castanzo, D.T., Chowdhury, S., Stjepanovic, G., Stefely, M.S., Hurley, J.H., Lander, G.C., Martin, A., 2018. The peroxisomal AAA-ATPase Pex1/Pex6 unfolds substrates by processive threading. Nat Commun 9, 135.
[56] Fujiki, Y., Okumoto, K., Honsho, M., Abe, Y., 2022. Molecular insights into peroxisome homeostasis and peroxisome biogenesis disorders. Biochim Biophys Acta Mol Cell Res 1869, 119330.
[57] Zhao, H.D., Li, C.X., Naik, M.Y., Wu, J., Cardilla, A., Liu, M., Zhao, F.R., Snyder, S. A., Xia, Y., Su, G.Y., Fang, M.L., 2023. Liquid Crystal Monomer: A Potential PPARγ Antagonist. Environ Sci Technol 57, 3758–3771.
[58] Amani, J., Gorjizadeh, N., Younesi, S., Najafi, M., Ashrafi, A.M., Irian, S., Gorjizadeh, N., Azizian, K., 2021. Cyclin-dependent kinase inhibitors (CDKIs) and the DNA damage response: The link between signaling pathways and cancer. DNA Repair 102, 103103.
[59] Pellarin, I., Dall'Acqua, A., Favero, A., Segatto, I., Rossi, V., Crestan, N., Karimbayli, J., Belletti, B., Baldassarre, G., 2025. Cyclin-dependent protein kinases and cell cycle regulation in biology and disease. Signal Transduct Target Ther 10.
[60] Cheng, H., Zhang, N., Pati, D., 2020. Cohesin subunit RAD21: From biology to disease. Gene 758, 144966.
[61] Wang, B., Wang, Y., Zhang, J., Hu, C., Jiang, J., Li, Y., Peng, Z., 2023. ROS-induced lipid peroxidation modulates cell death outcome: mechanisms behind apoptosis, autophagy, and ferroptosis. Arch Toxicol 97, 1439–1451.
[62] Huang, W., Yin, H., Yang, Y., Jin, L., Lu, G., Dang, Z., 2021. Influence of the co-exposure of microplastics and tetrabromobisphenol A on human gut: Simulation in vitro with human cell Caco-2 and gut microbiota. Sci Total Environ 778, 146264.
[63] Fan, Y., Lei, Z., Huang, J., Su, D., Ni, D., Chen, Y., 2023. Effect and mechanism of theaflavins on fluoride transport and absorption in Caco-2 cells. Foods 12, 12071487.
[64] Qu, T.J., Sun, Q., Tan, B., Wei, H., Qiu, X.X., Xu, X.J., Gao, H., Zhang, S., 2025. Integration of network toxicology and transcriptomics reveals the novel neurotoxic mechanisms of 2, 2′, 4, 4′-tetrabromodiphenyl ether. J Hazard Mater 486, 136999.